

Electronic and optical excitations of the PTB7 crystal: First-principles GW-BSE calculationsLong-Hua Li,^{*} Oleg Y. Kontsevoi, and Arthur J. Freeman*Department of Physics and Astronomy, Northwestern University, Evanston, Illinois 60208-3112, USA*

(Received 2 June 2014; published 10 November 2014)

Given the recent success in achieving efficient organic photovoltaic solar cells based on thieno[3,4-b]thiophene/benzodithiophene polymers (PTB7) and growing efforts to further improve the power conversion efficiency of the PTB7-based devices, a detailed atomic-scale picture of the electronic structure and the excitonic properties of PTB7 crystal is highly desirable. We report electronic and optical properties of PTB7 on the basis of first-principles density functional theory and GW many-body plus Bethe-Salpeter equation (GW-BSE) calculations. It is established that the first two highest valence bands (HVBs) and the first two lowest conduction bands (LCBs) originate from the benzodithiophene and thieno[3,4-b]thiophene functional units, respectively, thus confirming the donor-acceptor nature of PTB7. A significant difference of band splitting between HVBs and LCBs is found and its origins are explained. Our results strongly suggest that the strength of the interchain π - π interaction is not only a function of interchain distance, but is also highly dependent on the nature of the fused rings. The experimental optical absorption spectrum of PTB7 is well reproduced and explained by our GW-BSE calculations. Further analysis shows that the nature of the lowest singlet (triplet) excitons in polymeric crystals such as PTB7 differs from that of organic molecular crystals. A possible reason is explored by combining BSE calculations with a simple Hamiltonian model.

DOI: [10.1103/PhysRevB.90.195203](https://doi.org/10.1103/PhysRevB.90.195203)

PACS number(s): 71.35.Cc, 71.20.Rv, 71.15.Mb, 88.40.H-

I. INTRODUCTION

There is increasing research interest in π -conjugated organic oligomers and polymers due to their potential applications for molecular materials based electronic and optoelectronic devices, such as organic photovoltaic (OPV) cells [1–3]. Among those, the donor-acceptor (D-A) copolymers, which integrate electron-rich (donor) and electron-poor (acceptor) functional groups within the single repeating unit, are receiving growing attention [4–6]. In the D-A polymers, the highest occupied molecular orbital (HOMO) is usually located at the donor unit and the lowest unoccupied molecular orbital (LUMO) is at the acceptor unit, which creates an efficient strategy for tuning both HOMO and LUMO separately, as well as to modulate the electronic and optoelectronic properties. In the last few years, a new class of D-A heteroconjugated polymers with benzodithiophene (BDT) and thieno[3,4-b]thiophene (TT) alternating units exhibiting superior solar energy power conversion efficiency (PCE) has been developed [7]. Since different types of alkyl side chains can be attached to some positions of the backbone of poly-thienothiophene-benzodithiophene (PTB), these serial polymers were named PTB n ($n = 1 - 7$) [8,9]. Among these polymers, thieno[3,4-b]thiophene/benzodithiophene polymer PTB7, which has 2-ethylhexyl appended at TT and 2-ethylhexyloxy at BDT, exhibits the highest PCE of about 8% [9–11]. Despite significant progress made in the device performance of PTB-based OPV cells, a number of fundamental questions still remain open at the atomic and electronic level. For example, the crystal structure of the polymer is not well characterized experimentally and has not been assessed theoretically, and the details of the electronic band structure are not known. In particular, as a photoactive material, its optical absorption spectrum has been measured; however, the

nature of the optical transitions and excitons are far from being understood.

In general, for molecular crystals formed from small organic molecules, the lowest exciton is always strongly confined on a single molecule—the so-called Frenkel (FR) type exciton [12,13]—because the effective interactions of excited electron-hole (e - h) pairs between single molecules are weak [14]. However, for a polymeric crystal, the backbone is extended in one direction and the interaction between two chains is likely to increase due to the extent of π states. Such a dimensionality and the π - π stacking interaction may cause excited e - h pairs to distribute among the backbones to some degree, i.e., the excitons may exhibit the charge transfer (CT) feature [14,15]. Therefore, the quantitative insight from electronic structure calculations is of fundamental importance for clarifying and understanding the nature of optical excitations in D-A type polymers.

One successful way to obtain the optical excitation properties from first principles is the GW approximation together with the Bethe-Salpeter equation (GW-BSE) approach [16,17], in which many-body effects are considered, such as the electron-electron (e - e) and electron-hole (e - h) interactions. The GW-BSE-based methods have been applied with success to electronic and optical excitations of organic molecules and oligomers in the past decade [14,15,18–29]. Previous GW-BSE studies on oligomers have demonstrated size dependence of their optical properties [19]. However, this type of research on extended organic systems, such as polymeric crystals, is relatively limited [30–35]. Although a trend of increased probability of CT excitons for polymers can be deduced from pioneering studies on molecules and oligomers [14,19–21] the competition between FR and CT due to e - h interaction is still not well understood in polymeric crystals.

In this work, we investigate the electronic and optical properties of PTB7 based on the first-principles GW approximation and BSE calculations. The calculated optical spectra are described and compared with available experimental data.

^{*}longhua.li@northwestern.edu

We present here a more profound explanation of the electronic structure, optical absorption spectrum, and exciton properties of PTB7 which may help to optimize the interchain interactions in D-A polymers design.

II. MODELS AND COMPUTATIONAL METHOD

Our computational approach is as follows. First, structure optimization calculations are performed by the VASP code [36] in the framework of density functional theory (DFT). The plane wave basis with the frozen-core projector augmented wave [37,38] potential and a plane wave cutoff energy of 600 eV are used for the unit cell optimization. The general gradient approximation functional of Perdew-Burke-Ernzerhof [39] is employed. In order to describe the long-range van der Waals (vdW) interactions, the vdW-DF functional proposed by Dion *et al.* [40] is used. The cell optimization is performed until the atomic forces on each atom are less than 0.005 eV/Å.

After the structure optimization, the electronic ground state calculations are carried out by the PWSCF code of the QUANTUM ESPRESSO [41] package. The Trouiller-Martins [42] type norm-conserving pseudopotentials with the local density approximation (LDA) are used to represent the core electrons and nuclei. The cutoff energy of 60 Ry is used for expanding the valence wave functions. The Brillouin zone integrals for the ground state calculation use $1 \times 4 \times 2$ Monkhorst-Pack sampling. The PWSCF-generated DFT-LDA eigenvectors and eigenvalues are then used in the quasiparticle (QP) energy calculations with a single shot G_0W_0 approximation as implemented in the YAMBO [43] code. The dynamic screened interactions are described within the plasmon pole approximation [44]. After the static inverse dielectric function within the random-phase approximation (RPA) [45] is calculated, the neutral excitation energies and spectra are obtained by solving the BSE in the effective two-particle Schrödinger equation [46–48]:

$$H_{vck,v'c'k'}^{\text{exc}} A_{vck}^s = E^{\text{exc}} A_{v'c'k'}^s, \quad (1)$$

where H^{exc} is the excitonic Hamiltonian and A^s and E^{exc} are the excited eigenfunctions and eigenvalues. The excitonic Hamiltonian is defined as

$$H^{\text{exc}} = \begin{pmatrix} H^{\text{res}} & H^{\text{cpl}} \\ -[H^{\text{cpl}}]^* & -[H^{\text{res}}]^* \end{pmatrix}, \quad (2)$$

where H^{res} and H^{cpl} are the resonant term and the coupling term. The resonant part,

$$H_{vck,v'c'k'}^{\text{res}} = (E_{ck} - E_{vk})\delta_{vv'}\delta_{cc'}\delta_{kk'} + 2\nu_{vck}^{v'c'k'} - W_{vck}^{v'c'k'}, \quad (3)$$

is Hermitian, where c and v are the indices of the conduction and the valence bands, respectively, and k is the k vector. The first part of this Hamiltonian is analogous to the single-particle Hamiltonian and the last two parts compose the BSE kernel. The eigenvalues, ε , can be obtained from LDA or GW calculations. The e - h effects are mainly determined by the repulsive exchange e - h interaction 2ν and the attractive e - h interaction W . In principle, the influence of the e - h interaction on the optical absorption could be explored by including only 2ν , or only W , or both of them in the optical calculations. Usually, the coupling term H^{cpl} is ignored to simplify the calculation, which is referred to as the Tamm-Dancoff approximation (TDA) [49]. Because the errors introduced by the TDA are

still under discussion [23,50], we include the coupling term in the excitonic Hamiltonian to eliminate these errors. Test calculations show that a k -point sampling density of $2 \times 8 \times 4$ and 300 conduction bands in the G_0W_0 calculations converge the band gap within 80 meV. For the diagonalization of the BSE Hamiltonian, ten conduction and ten valence bands are found to be sufficient to achieve a converged spectrum.

III. RESULTS AND DISCUSSION

A. Geometry structure

The monomer of PTB7 contains four main structural parts as shown in Fig. 1. The backbone consists of TT and BDT, and the side chains are three similar alkyl chains, namely, two 2-ethylhexyl (2-EH) chains on BDT and one 2-ethylhexyloxy (2-EHO) chain on TT. The starting crystal model was built from two chains stacked on top of each other along the b axis forming a π - π stacking between the similar thiophene units, i.e., TT-TT and BDT-BDT. The optimized crystal symmetry of PTB7 is triclinic with the following structural parameters: $a = 22.83$ Å, $b = 8.49$ Å, $c = 12.27$ Å, $\alpha = 95.08^\circ$, $\beta = 93.69^\circ$, and $\gamma = 87.77^\circ$. The average π - π stacking distance is 3.81 Å, which is close to the experimental value of 3.79 Å [9]. Because of relatively low crystallinity of PTB7 [9], its full crystal structure is not yet resolved experimentally. The π - π stacking distance is the one calculated structural feature that can be compared with experiment at present, and the comparison is favorable. It was found that the backbone tilt occurs after the relaxation, which is common in other thiophene systems such as P3HT [51] and PBTTT [52]. The backbone tilt angles are defined as the angles between the plane of the respective backbone thiophene unit, TT or BDT, and the a axis (Fig. 1, θ_{BDT} and θ_{TT}). It is interesting to see

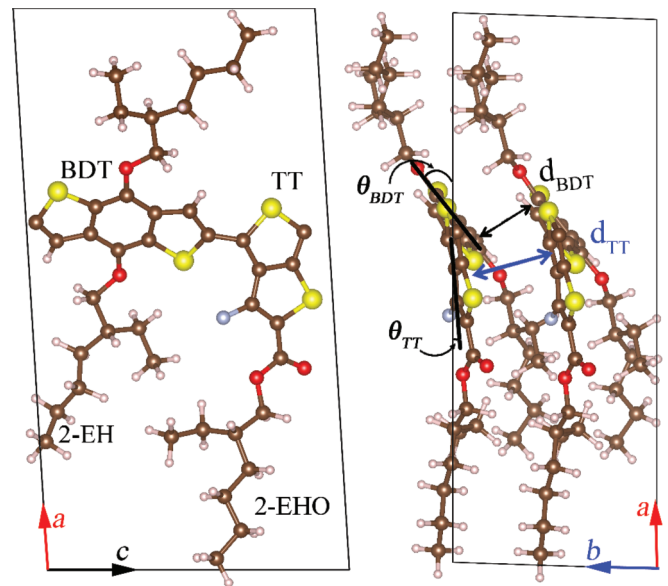


FIG. 1. (Color online) PTB7 crystal structure after full relaxation. The d_{BDT} and d_{TT} are the intermolecular π - π stacking distances between BDT-BDT and TT-TT, respectively; θ_{BDT} and θ_{TT} are the tilt angles of BDT and TT, respectively. Colors of atoms are S, yellow; C, brown; O, red; F, light blue; and H, pink.

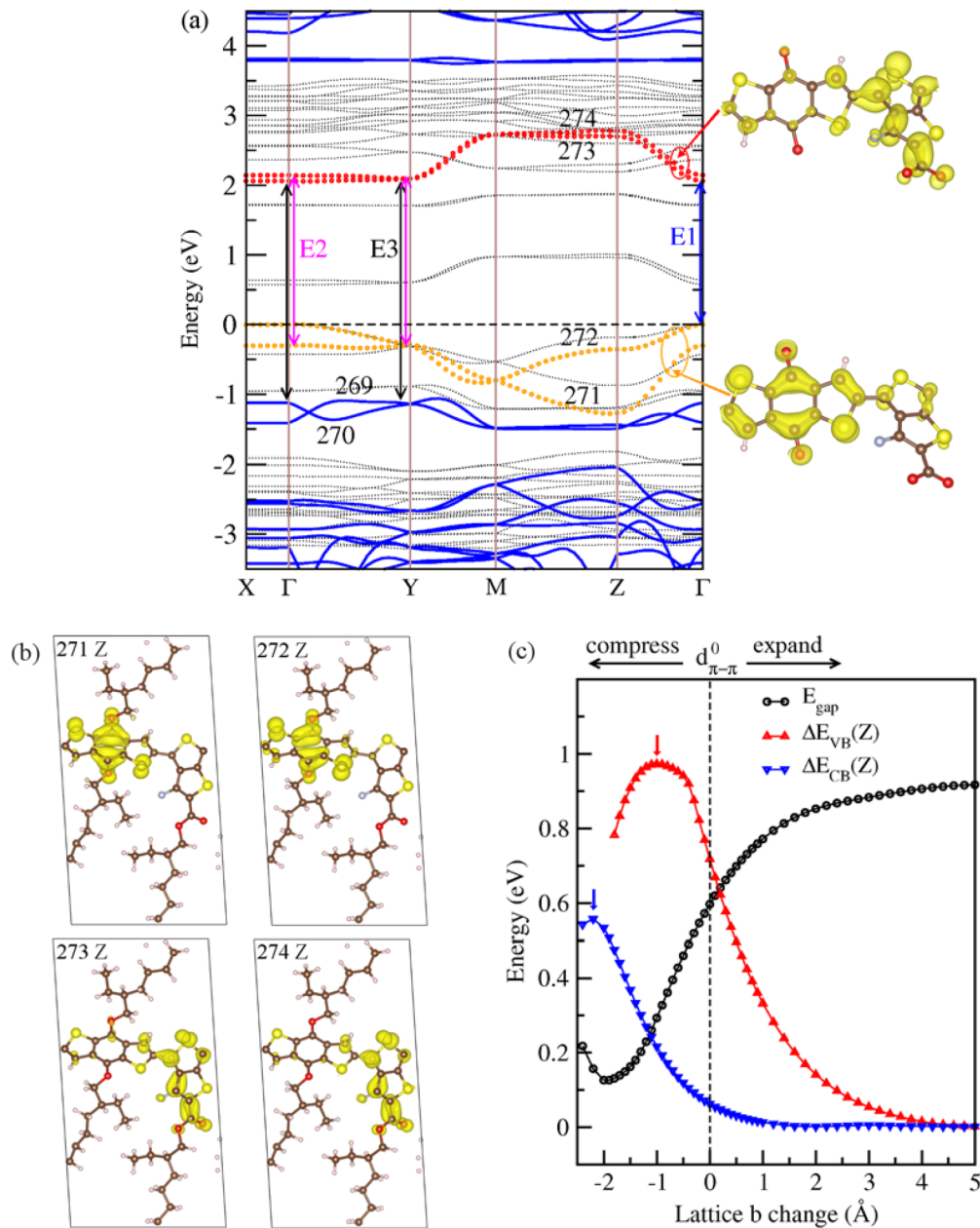


FIG. 2. (Color online) (a) LDA (black dots) and G_0W_0 (color lines) band structures of PTB7; the two LCBs and the four HVBs are labeled by the corresponding band numbers; the main interband transitions are marked by arrows. On the right, electronic charge densities of two HVBs (bottom) and two LCBs (top); only the backbone is shown; isosurface level is 0.003 bohr^{-3} . (b) Electronic charge density of the two lowest CBs and two highest VBs at Z; isosurface level is 0.0001 bohr^{-3} . (c) The dependence of the band gap and the band splitting of the two lowest CBs and two highest VBs at Γ and Z on the changes of the lattice parameter b ; the dashed line corresponds to the equilibrium structure.

that the tilt of BDT is larger than that of TT: the BDT tilt angle is about 30° , while the tilt of TT is much smaller, about 5° , and is almost unchanged by the structural relaxation. The calculated π - π stacking distances are also different for TT-TT and BDT-BDT: 4.11 \AA for d_{TT} , and 3.51 \AA for d_{BDT} . One possible reason for these differences in tilt angle and π - π stacking distances is that BDT has three fused heterocyclic rings for which the π - π stacking interactions are stronger than that between TT with two fused heterocyclic rings. Stronger interactions result in a decrease of the π - π stacking distance for BDT-BDT, while tilting allows compensating for the π - π stacking distance differences.

B. Electronic structure

In order to understand the origin of the difference in the π - π interaction between BDT-BDT and TT-TT, we investigate the relationship between the electronic properties and the interchain interaction of PTB7. Moreover, a detailed and quantitative description of the electronic band structure is necessary for the interpretation of optical absorption obtained experimentally.

In Fig. 2(a), the calculated LDA and G_0W_0 band structures of PTB7 are presented for comparison in order to exhibit the many-body effects on the electronic bands. The black dotted lines are the LDA bands, and the G_0W_0 bands are

given in color. The first two highest valence bands (HVBs), bands 271 and 272, and the first two lowest conduction bands (LCBs), bands 273 and 274, are marked by the orange and red dots, respectively, on the G_0W_0 band structure plot. The G_0W_0 quasiparticle corrections (QPCs) open the band gap dramatically by about 1.5 eV compared to the LDA gap. It can be also seen that the QPC is not a simple scissor operation on the LDA band structure: The strength of the QPC varies significantly with different crystal axis directions. This emphasizes the importance of using the G_0W_0 band structure for optical calculations instead of the LDA band structure. According to the PTB7 crystal structure, the electronic bands associated with the interchain interaction are in the Γ - Z direction while the bands associated with the intrachain interaction are along the Γ - Y line. To evaluate the character of the HVBs and LCBs, the charge densities for bands 271, 272, 273, and 274 were calculated and are shown on the right-hand side of Fig. 2(a). It can be seen that the first two HVBs and the first two LCBs are dominated by the backbone Cp_z-Cp_z orbital interactions, forming the p_π or p_{π^*} orbitals. In the Green's function approach, a quasiparticle is an electron plus its surrounding screening cloud, and the QP energy is related to the energy needed to add (remove) an electron to (from) the system [49]. This means that large electric screening results in less energy correction to the Kohn-Sham (KS) energy due to a high energy barrier for adding or removing an electron from a KS orbital. Since the screening (overlap) of p_π orbitals is smaller for the interchain π - π stacking direction (b axis) than that for the intrachain π - π interaction direction (c axis), the QPCs for the bands along the Γ - Z direction are larger than for the Γ - Y direction. This is the reason that the energy difference between LDA and G_0W_0 bands is larger at the Z k point than at the Y point. It also illustrates the intrachain and interchain interaction effects on the electronic structure of the polymeric crystal.

An important consequence of the interchain interaction is the band splitting at Z . Although this band splitting is common in thin films of π -conjugated polymers, such as polythiophene [35] and PBTTT [52], it is particularly interesting to find out that in the PTB7 case the band splitting of the first two HVBs at Z [$\Delta E_{VB}(271, 272, Z)$] is significantly larger than the splitting of the first two LCBs [$\Delta E_{CB}(273, 274, Z)$]: 0.92 vs 0.06 eV, according to the G_0W_0 band structure. The question is then raised, what is the origin of the difference between ΔE_{VB} and ΔE_{CB} at Z ? To address this question directly, we analyze the charge densities of bands 271–274 at Z , which are presented in Fig. 2(b). It is evident that the charge densities of HVBs and LCBs are localized on different backbone parts: HVBs situate at the BDT unit, while LCBs at the TT. This result demonstrates that in the PTB7 polymer the BDT functional unit acts as a donor and the TT unit is an acceptor. We can then interpret this discrepancy between ΔE_{VB} and ΔE_{CB} at Z as a consequence of different strengths of interchain interactions between BDT-BDT and TT-TT. The fact that the splitting $\Delta E_{VB}(Z)$ is larger than $\Delta E_{CB}(Z)$ demonstrates that the BDT-BDT interaction is stronger than the TT-TT interaction. This result confirms the assessment made in Ref. [9] on the basis of experimental observations that the BDT units have stronger π - π interactions.

In order to further understand the nature of the difference between BDT-BDT and TT-TT interactions, the dependence

of the band splitting on the interchain π - π stacking distance was calculated by varying the lattice parameter b , and is presented in Fig. 2(c). All band energies are obtained from LDA calculations, therefore band splitting and the band gaps are underestimated in Fig. 2(c) due to the absence of G_0W_0 quasiparticle corrections, but the trends should remain the same. The dashed line corresponds to the equilibrium structure in which the π - π stacking distance d° for BDT-BDT and TT-TT are 3.5 and 4.1 Å, respectively. The band splittings and the band gap are nonlinearly dependent on the interchain distance. The increase of the interchain distance results in the decrease of band splitting for both $\Delta E_{VB}(Z)$ and $\Delta E_{CB}(Z)$ until the splitting reaches zero at 5 Å of lattice expansion indicating that the interchain interaction vanishes and the HVBs and LCBs become degenerate. On the other hand, the compression of the b lattice parameter leads to an increase of the band splitting for $\Delta E_{VB}(Z)$ and $\Delta E_{CB}(Z)$ until it reaches a maximum. However, at any point $\Delta E_{CB}(Z)$ is smaller than $\Delta E_{VB}(Z)$. This result proves that the BDT-BDT interaction is intrinsically stronger than the TT-TT interaction. The reason for this is not only due to the number of fused rings (three rings in BDT vs two rings in TT), but also results from the stronger π conjugation of the six π electrons in the benzene ring. This is only present in BDT, compared to the 5π -electron conjugation in the thiophene rings. It can be deduced from Fig. 2(b) that significantly more π -electron density localizes on the benzene ring than on the thiophene rings. Thus, our calculations strongly suggest that the band splitting is not only determined by the π - π stacking distance, but also by the nature of the backbone itself, which is related to the strength of the π conjugation. Now, we propose that one of the possible reasons that PTB7 does not have a high degree of crystallinity in thin films [9] is likely due to the significant difference of the equilibrium π - π stacking distance between BDT-BDT and TT-TT, or the difference of the π conjugation strength between BDT and TT. Improvement in the performance of PTB-based OPV devices could be achieved by enhancing the ordering and the π - π interaction of the backbone. This is because stronger π -stacking interactions often lead to higher charge transport [5,6], an important factor impacting OPV efficiency. According to our calculations, TT is not a very good acceptor from the point of view of the interchain π - π interaction alone. We suggest introducing benzene rings in future D-A polymer designs in order to enhance the interchain π - π interaction. Another possible way to improve π - π interactions is to use linear and short side chains, because both experiments [9,53] and theoretical calculations [52] indicate that branching of side chains could substantially increase π - π stacking distances and decrease the π - π interaction.

C. Optical excitations

We now focus on the optical properties of PTB7. The many-body e - h effects will be briefly described and we will then compare our calculated optical spectrum with the experimental one. The optical dipole transitions will be analyzed and discussed thoroughly. Finally, we will discuss the nature of the difference between excitons in polymeric crystals versus small molecular crystals.

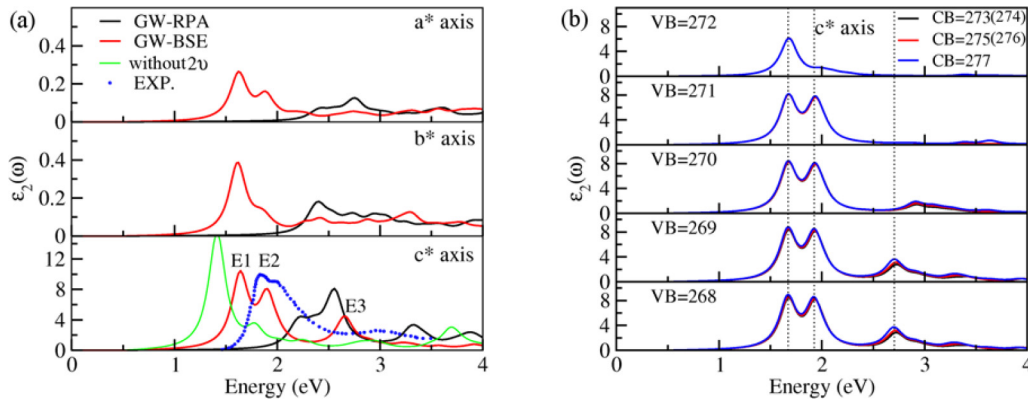


FIG. 3. (Color online) (a) Calculated imaginary part of the dielectric function $\epsilon_2(\omega)$ along the three reciprocal lattice axes: black line, RPA; red line, BSE; green line, the BSE calculation without the exchange e - h interaction 2ν ; blue dots, experimental data from Ref. [33]. E_1 , E_2 , and E_3 mark the three excitonic peaks on the BSE spectrum. (b) Band decomposition of $\epsilon_2(\omega)$ in the BSE calculations.

The calculated imaginary parts (ϵ_2) of the dielectric function along the three reciprocal lattices a^* , b^* , and c^* for PTB7 are summarized in Fig. 3(a). The e - h effects to the optical absorption are analyzed by comparing the RPA and BSE results. The first three optical transition peaks are located at 2.23, 2.56, and 3.34 eV in the GW-RPA calculation, while in the GW-BSE the first three peaks are located at 1.64, 1.90, and 2.67 eV. The e - h interaction induces not only a redshift of the optical transition energies, but also an enhancement of the absorption oscillator strengths, especially for the first optical transition peak E_1 . Because significant oscillator strengths are only exhibited along the c^* axis, which is the backbone direction, we will analyze the light polarized spectrum along this direction in more detail.

It is straightforward to compare our calculated spectrum with the measured optical absorption spectrum. The experimental spectrum exhibits three main peaks [7,8,10,54] [Fig. 3(a), the blue dotted line], which is in agreement with our GW-RPA and GW-BSE calculations. Since the photon energies of those three peaks are very similar in Refs. [7,8,10,39,54], only the latest experimental spectrum from Ref. [33] is shown in Fig. 3(a) for comparison. The three experimental peaks are located at about 680, 615, and 420 nm [54], which correspond to 1.82, 2.01, and 2.95 eV. The GW-BSE spectrum is more consistent with the experimental one than the GW-RPA calculation when considering the relative oscillator strengths of peaks E_1 and E_2 . The main discrepancy between the GW-BSE calculated $\epsilon_2(\omega)$ and the experimental spectrum is the redshift by 0.2 eV of the main absorption bands in the calculated spectrum compared with the experimental one. This difference is likely due to the underestimation of the G_0W_0 quasiparticle band gap, which may be caused by the plasmon pole approximation and the use of LDA wave functions for quasiparticle energy calculations, as well as by an insufficient number of k points and unoccupied bands. In addition to that, a recent study [27] suggests that the GW bulk band gap can be lower than the surface band gap by 0.2–0.4 eV in organic semiconductors due to reduced polarization on the surface. Because the experimental spectrum was measured for a PTB7 film rather than bulk material, the redshift of our GW-BSE calculated spectra is reasonable. Also, a small discrepancy of the optical band splitting is found between

the GW-BSE calculation and the experimental spectrum, 0.26 vs 0.19 for $\Delta_{E_1E_2} = E_2 - E_1$, and 0.76 vs 0.94 eV for $\Delta_{E_2E_3} = E_3 - E_2$. This is most likely related to some differences in the crystal structure between our model and the experiment and due to the presence of disorder in the experimental samples, since the band splitting is strongly dependent on the π - π stacking, as we discussed earlier. Overall, our GW-BSE spectrum agrees well with the measured optical absorption spectrum.

In order to understand the origins of the peaks in the optical absorption spectrum in experiment, we calculate $\epsilon_2(\omega)$ by increasing step by step the number of valence bands as well as conduction bands in the BSE Hamiltonian (1). It can be seen in the lower panel of Fig. 3(b) that the two lowest conduction bands and four highest valence bands are sufficient to achieve a rather converged BSE spectrum. In addition, our results demonstrate that the first exciton peak, E_1 , is dominated by the transitions between the highest valence band 272 and the lowest conduction band 273 [Fig. 3(b), upper panel]. The second peak, E_2 , is the result of the interband transition between the second highest valence band 271 and the two lowest conduction bands. The third peak, E_3 , is due to the transitions from the third and fourth valence bands, 269 and 270. The detailed explanations of band transitions $E_1 - E_3$, which are labeled in Fig. 2(a), are obtained by analyzing the states contributing to the absorption peaks according to the method of Ref. [35]. The first absorption peak E_1 is mostly contributed from the band-to-band transition between 272 and 273 at Γ , i.e., the HOMO-LUMO transition. The E_2 is ascribed to the interband transition between 271–274 and 272–274 around Γ and Y . The interband transitions between 269–273 together with 270–273 around Γ and Y are the main contributions to E_3 . These results are consistent with the band-by-band decomposition in Fig. 3(b).

Finally, we explore the nature of the excitons in the PTB7 crystal. The electronic charge distributions for the three absorption peaks are shown in Fig. 4. The hole is located on BDT due to its donor nature, as shown by the arrows in Fig. 4. All three absorption peaks are found to be a mixture of the Frenkel and the charge transfer excitons where the hole and a part of the electrons are localized at the same chain, while other electrons localize at different chains. However, the electronic

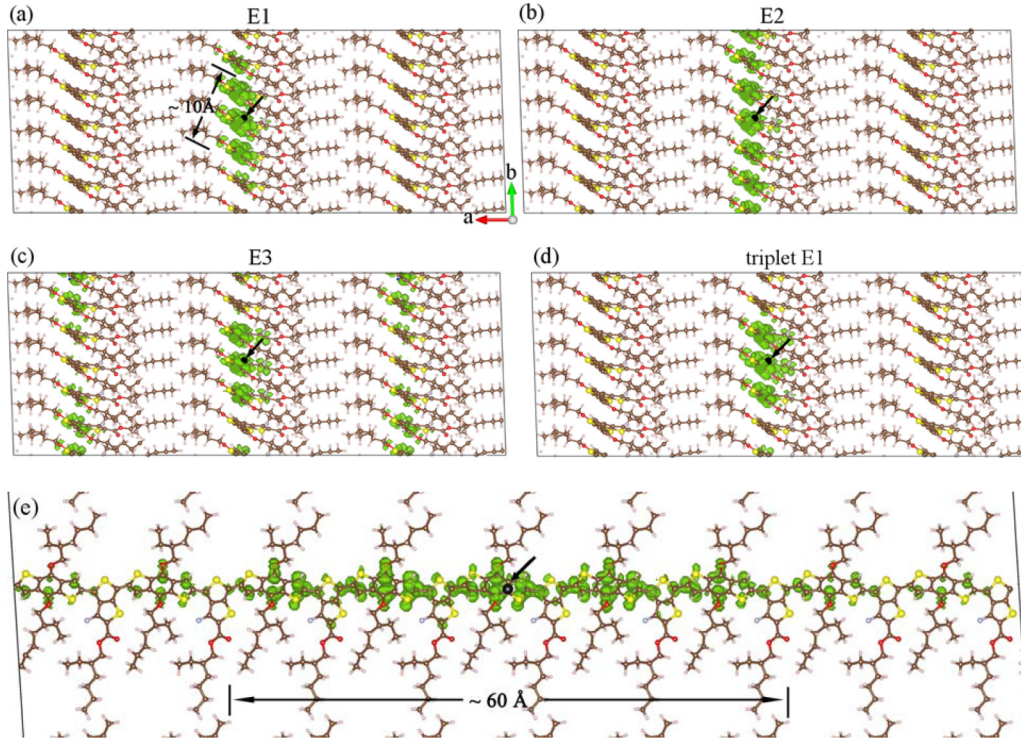


FIG. 4. (Color online) Electronic charge distribution around the hole on BDT (black dot, pointed to by the arrow) for (a)–(c) three spin singlet excitons, and (d) the lowest spin triplet exciton. (e) Excitation distribution of $E1$ along the c axis. Isosurface value is 0.01 bohr^{-3} .

distributions are quite different among the three excitons. The lowest bound exciton $E1$ is restricted to only a few chains along the stacking direction (b axis), while the second bound exciton $E2$ is significantly more extended along the interchain π - π stacking direction. In contrast, the distribution of the third exciton, the resonant exciton $E3$, is instead extended in the lamellar direction (a axis). In addition, Fig. 4(e) shows that the lowest bound exciton $E1$ has an extended distribution along the backbone (c axis): Its size is about five unit cell lengths ($\sim 60 \text{ \AA}$) in this direction, which is much larger than its extension of only two to three π - π stacking distances ($\sim 10 \text{ \AA}$) along the b axis shown in Fig. 4(a). The nature of these three excitons indicates that the first two bound excitons may be affected by the interchain distance, and the third exciton may be influenced by the change of morphology in the lamellar direction. As expected, the nature of the lowest bound exciton of PTB7 is totally different from organic molecular crystals in which the lowest absorption peak often corresponds to the Frenkel type exciton [12]. Interestingly, the lowest triplet exciton still shows the CT character [Fig. 4(d)] for PTB7. This is also apparently different from organic molecular crystals. According to current research [14,18] the lowest excited state in the triplet channel is generally an FR excitation in molecular solids. The reason for the discrepancy of the lowest spin singlet (triplet) exciton between polymeric and molecular crystals can be interpreted as follows. The excitonic energies for FR and CT excitons can be expressed as [14,18] $E^{\text{FR}} = \Delta\varepsilon_0 + \bar{v} - \ddot{W}$, and $E^{\text{CT}} = \Delta\varepsilon_0 - \hat{W}$, where $\Delta\varepsilon_0$ is the band gap, \ddot{W} and \hat{W} are the on-site attractive and the intersite attractive e - h interactions, respectively, and \bar{v} is the repulsive e - h interaction. For molecular crystals, the on-site attractive e - h

is much stronger than the intersite attractive matrix element \hat{W} between two molecules. Thus, the relative magnitude of E^{FR} and E^{CT} is determined by the relationship of the repulsive e - h interaction \bar{v} and the on-site attractive e - h interaction \ddot{W} . The E^{FR} is much lower than the E^{CT} in the spin triplet channel ($\bar{v} = 0$), because $\ddot{W} \gg \hat{W}$, therefore the lowest triplet exciton is predominantly a FR exciton in molecular crystals. However, whether the lowest singlet exciton is CT or FR depends on the relative strength of \bar{v} and \ddot{W} , e.g., FR for picene [14] but a mixture of CT and FR for pentacene [14,26,27] and perylene-3,4,9,10-tetracarboxylic dianhydride [27,55]. For the PTB7 crystal, the on-site attractive e - h interaction \ddot{W} may be close to the sum of intersite attractive matrix elements \hat{W} due to the strong interchain π - π interaction. Thus, the strength of \bar{v} is critical to the energy difference between E^{FR} and E^{CT} . If \bar{v} is not strong, E^{FR} is then close to E^{CT} , and the lowest singlet exciton is a mixture of CT and FR. In fact, our calculations confirmed that 2ν yields only a small contribution to the energy of $E1$. This conclusion was reached by diagonalizing the excitonic Hamiltonian (1) in which the repulsive exchange e - h interaction 2ν is removed. The results [Fig. 3(a), green line] indicate that the attractive W strongly contributes to the $E1$ whereas the repulsive 2ν contributes mostly to the excitonic energies and the oscillator strengths of $E2$ and $E3$. Therefore, the fact that the direct e - h interaction W is stronger than the repulsive exchange 2ν is the main reason for the lowest singlet exciton being the mixture of FR and CT. This agrees well with the above analysis of the Hamiltonian model. Obviously, as \ddot{W} is close to \hat{W} in the PTB7 polymer, i.e., $E^{\text{FR}} \approx E^{\text{CT}}$, the lowest triplet is still the mixed type of exciton for PTB7. These results may be extended to other polymeric crystals, i.e., in a

polymeric crystal both the lowest singlet and triplet excitons are likely to exhibit CT character. It also indicates that the exciton binding energy in a polymeric crystal should always be smaller than in an organic molecular crystal due to the CT character of excitons in a polymeric crystal and FR character of excitons in a molecular crystal. Our results demonstrate the relation between the exciton properties and the direct e - h interaction W , i.e., the interchain π - π interaction. This is consistent with previous works [18,19,21,22] on organic molecular and polymeric crystals and shows that the exciton binding energy is dependent on the molecular size and on the intermolecular interactions.

IV. CONCLUSIONS

In summary, the crystal structure, electronic band structure, and optical properties of PTB7 crystal were investigated on the basis of first-principles DFT and many-body GW-BSE calculations. It was established that the two HVBs (HOMO) originate from the BDT functional unit, while the two LCBs (LUMO) are localized at the TT unit. This confirms that PTB7 is a D-A polymer and BDT acts as a donor and TT is an acceptor. The analysis of the relaxed structure and electronic charge densities suggest that the BDT-BDT stacking has stronger π - π interactions than the TT-TT stacking, which is in agreement with experimental observations. The stronger BDT-BDT than the TT-TT interaction leads to a significantly larger band splitting of HVBs at the Z k point than that of LCBs. We found that the origin of the strong BDT-BDT π - π interaction comes from the 6 π -electron benzene ring in BDT. The results demonstrate that the strength of the interchain

interaction is determined by the π conjugation of the fused Rings. The GW-BSE calculated optical spectrum is in good agreement with the measured optical absorption spectrum. The origins of the main peaks in the optical absorption spectrum are understood: The first absorption peak is from the HVB to LCB transition, the second peak is from HVB and HVB-1 to LCB+1 transitions, and the third peak is due to HVB-2 and HVB-3 to LCB transitions. Moreover, our results indicate that the nature of the lowest singlet (triplet) excitons in polymeric crystals and organic molecular crystals may be significantly different. For a molecular crystal, the lowest triplet exciton is often the FR type, while the type of the lowest singlet depends on the relative strength of the on-site repulsive and attractive e - h interaction. For PTB7 or a polymeric crystal, both the lowest singlet and triplet excitons are FR mixed with CT type excitons. The analysis of a simple Hamiltonian model suggests that the small contribution of the repulsive exchange e - h interaction is the main condition that results in the lowest singlet exciton being a mixed type exciton for the PTB7 crystal, which is consistent with our BSE calculations.

ACKNOWLEDGMENTS

This work was supported by the Argonne-Northwestern Solar Energy Research (ANSER) Center, an Energy Frontier Research Center funded by the U.S. Department of Energy, Office of Science, and Office of Basic Energy Sciences under Award No. DE-SC0001059. Computing resources were provided by the National Energy Research Scientific Computing Center, a DOE Office of Science User Facility supported by the Office of Science of the U.S. Department of Energy under Contract No. DE-AC02-05CH11231.

-
- [1] C. J. Brabec, N. S. Sariciftci, and J. C. Hummelen, *Adv. Funct. Mater.* **11**, 15 (2001).
- [2] K. M. Coakley and M. D. McGehee, *Chem. Mater.* **16**, 4533 (2004).
- [3] Y. Li, *Acc. Chem. Res.* **45**, 723 (2012).
- [4] Z.-G. Zhang and J. Wang, *J. Mater. Chem.* **22**, 4178 (2012).
- [5] X. Guo, H. Xin, F. S. Kim, A. D. T. Liyanage, S. A. Jenekhe, and M. D. Watson, *Macromolecules* **44**, 269 (2010).
- [6] E. Ahmed, F. S. Kim, H. Xin, and S. A. Jenekhe, *Macromolecules* **42**, 8615 (2009).
- [7] Y. Y. Liang, D. Q. Feng, Y. Wu, S. T. Tsai, G. Li, C. Ray, and L. P. Yu, *J. Am. Chem. Soc.* **131**, 7792 (2009).
- [8] Y. Y. Liang and L. P. Yu, *Acc. Chem. Res.* **43**, 1227 (2010).
- [9] J. M. Szarko, J. C. Guo, Y. Y. Liang, B. Lee, B. S. Rolczynski, J. Strzalka, T. Xu, S. Loser, T. J. Marks, L. P. Yu, and L. X. Chen, *Adv. Mater.* **22**, 5468 (2010).
- [10] J. M. Szarko, J. C. Guo, B. S. Rolczynski, and L. X. Chen, *J. Mater. Chem.* **21**, 7849 (2011).
- [11] Y. Y. Liang, Z. Xu, J. B. Xia, S. T. Tsai, Y. Wu, G. Li, C. Ray, and L. P. Yu, *Adv. Mater.* **22**, E135 (2010).
- [12] V. M. Agranovich, *Excitations in Organic Solids* (Oxford University Press, New York, 2008).
- [13] V. M. Agranovich and V. L. Ginzburg, *Crystal Optics with Spatial Dispersion, and Excitons* (Springer, Berlin/Heidelberg, 1984).
- [14] P. Cudazzo, M. Gatti, and A. Rubio, *Phys. Rev. B* **86**, 195307 (2012).
- [15] M. L. Tiago, J. E. Northrup, and S. G. Louie, *Phys. Rev. B* **67**, 115212 (2003).
- [16] L. Hedin, *Phys. Rev.* **139**, A796 (1965).
- [17] E. E. Salpeter and H. A. Bethe, *Phys. Rev.* **84**, 1232 (1951).
- [18] P. Cudazzo, M. Gatti, A. Rubio, and F. Sottile, *Phys. Rev. B* **88**, 195152 (2013).
- [19] K. Hummer and C. Ambrosch-Draxl, *Phys. Rev. B* **71**, 081202(R) (2005).
- [20] K. Hummer, C. Ambrosch-Draxl, G. Bussi, A. Ruini, M. J. Caldas, E. Molinari, R. Laskowski, and N. E. Christensen, *Phys. Stat. Solidi B* **242**, 1754 (2005).
- [21] K. Hummer, P. Puschnig, and C. Ambrosch-Draxl, *Phys. Rev. Lett.* **92**, 147402 (2004).
- [22] K. Hummer, P. Puschnig, S. Sagmeister, and C. Ambrosch-Draxl, *Mod. Phys. Lett. B* **20**, 261 (2006).
- [23] M. Palummo, C. Hogan, F. Sottile, P. Bagala, and A. Rubio, *J. Chem. Phys.* **131**, 084102 (2009).
- [24] P. Puschnig and C. Ambrosch-Draxl, *Phys. Rev. B* **66**, 165105 (2002).
- [25] A. Riefer, E. Rauls, W. G. Schmidt, J. Eberhard, I. Stoll, and J. Mattay, *Phys. Rev. B* **85**, 165202 (2012).
- [26] F. Roth, B. Mahns, S. Hampel, M. Nohr, H. Berger, B. Buchner, and M. Knupfer, *Eur. Phys. J. B* **86**, 66 (2013).

- [27] S. Sharifzadeh, A. Biller, L. Kronik, and J. B. Neaton, *Phys. Rev. B* **85**, 125307 (2012).
- [28] C. Ambrosch-Draxl, D. Nabok, P. Puschnig, and C. Meisenbichler, *New J. Phys.* **11**, 125010 (2009).
- [29] N. Sai, M. L. Tiago, J. R. Chelikowsky, and F. A. Reboredo, *Phys. Rev. B* **77**, 161306(R) (2008).
- [30] P. Puschnig and C. Ambrosch-Draxl, *Phys. Rev. Lett.* **89**, 056405 (2002).
- [31] A. Ruini, M. J. Caldas, G. Bussi, and E. Molinari, *Phys. Rev. Lett.* **88**, 206403 (2002).
- [32] M. L. Tiago, M. Rohlfing, and S. G. Louie, *Phys. Rev. B* **70**, 193204 (2004).
- [33] J. W. van der Horst, P. A. Bobbert, M. A. J. Michels, G. Brocks, and P. J. Kelly, *Phys. Rev. Lett.* **83**, 4413 (1999).
- [34] G. Bussi, A. Ruini, E. Molinari, M. J. Caldas, P. Puschnig, and C. Ambrosch-Draxl, *Appl. Phys. Lett.* **80**, 4118 (2002).
- [35] J. W. van der Horst, P. A. Bobbert, and M. A. J. Michels, *Phys. Rev. B* **66**, 035206 (2002).
- [36] G. Kresse and J. Furthmuller, *Phys. Rev. B* **54**, 11169 (1996).
- [37] P. E. Blochl, *Phys. Rev. B* **50**, 17953 (1994).
- [38] G. Kresse and D. Joubert, *Phys. Rev. B* **59**, 1758 (1999).
- [39] J. P. Perdew, K. Burke, and M. Ernzerhof, *Phys. Rev. Lett.* **77**, 3865 (1996).
- [40] M. Dion, H. Rydberg, E. Schroder, D. C. Langreth, and B. I. Lundqvist, *Phys. Rev. Lett.* **92**, 246401 (2004).
- [41] P. Giannozzi, S. Baroni, N. Bonini, M. Calandra, R. Car, C. Cavazzoni, D. Ceresoli, G. L. Chiarotti, M. Cococcioni, I. Dabo *et al.*, *J. Phys.: Condens. Matter* **21**, 395502 (2009).
- [42] N. Troullier and J. L. Martins, *Phys. Rev. B* **43**, 1993 (1991).
- [43] A. Marini, C. Hogan, M. Gruning, and D. Varsano, *Comput. Phys. Commun.* **180**, 1392 (2009).
- [44] M. S. Hybertsen and S. G. Louie, *Phys. Rev. B* **34**, 5390 (1986).
- [45] H. Ehrenreich, *The Optical Properties of Solids* (Academic, New York, 1965).
- [46] S. Albrecht, L. Reining, R. Del Sole, and G. Onida, *Phys. Rev. Lett.* **80**, 4510 (1998).
- [47] L. X. Benedict, E. L. Shirley, and R. B. Bohn, *Phys. Rev. B* **57**, R9385 (1998).
- [48] M. Rohlfing and S. G. Louie, *Phys. Rev. Lett.* **81**, 2312 (1998).
- [49] G. Onida, L. Reining, and A. Rubio, *Rev. Mod. Phys.* **74**, 601 (2002).
- [50] P. Puschnig, C. Meisenbichler, and C. Draxl, [arXiv:1306.3790v2](https://arxiv.org/abs/1306.3790v2) [cond-mat.mtrl-sci].
- [51] T. Tsumuraya, J.-H. Song, and A. J. Freeman, *Phys. Rev. B* **86**, 075114 (2012).
- [52] L. H. Li, O. Y. Kontsevoi, S. H. Rhim, and A. J. Freeman, *J. Chem. Phys.* **138**, 164503 (2013).
- [53] C. Piliago, T. W. Holcombe, J. D. Douglas, C. H. Woo, P. M. Beaujuge, and J. M. J. Frechet, *J. Am. Chem. Soc.* **132**, 7595 (2010).
- [54] H. X. Wang, X. F. Yu, C. Yi, H. Ren, C. Liu, Y. L. Yang, S. Xiao, J. Zheng, A. Karim, S. Z. D. Cheng, and X. Gong, *J. Phys. Chem. C* **117**, 4358 (2013).
- [55] M. Hoffmann, K. Schmidt, T. Fritz, T. Hasche, V. M. Agranovich, and K. Leo, *Chem. Phys.* **258**, 73 (2000).